Interactive network of the dehydrogenation of alkanes, alkenes and alkynes – surface carbon hydrogenative coupling on Ru(111)

Yueyue Jiao[a,b,c], Huan Ma[a,b,c], Hui Wang[a,b,c], Yong-Wang Li[a,b,c,d] Xiao-Dong Wen*[a,b,c,d], and Haijun Jiao*[e]

(a) State Key Laboratory of Coal Conversion, Institute of Coal Chemistry, Chinese Academy of Sciences, Taiyuan 030001, P.R. China. (b) The University of Chinese Academy of Sciences, Beijing 100049, P.R. China. (c) National Energy Center for Coal to Liquids, Synfuels China Co., Ltd., Beijing 101400, P.R. China. (d) Beijing Advanced Innovation Center for Materials Genome Engineering, Industry-University Cooperation Base between Beijing Information S&T University and Synfuels China Co. Ltd, Beijing, China. (e) Leibniz-Institut für Katalyse e.V. an der Universität Rostock, Albert-Einstein Strasse 29a, 18059 Rostock, Germany: E-mails: wxd@sxicc.ac.cn; and Haijun.jiao@catalysis.de

Table S1. A cmparisition of the adsorption energy (eV) of CO*, CH$_4$*, CH$_3$CH$_3$*, CH$_3$CH$_2$CH$_{3*}$, CH$_3$*, CH$_3$CH$_2$*, and CH$_3$CH$_2$CH$_2$* on Ru(111) surface, and CO* on Ru(0001) surface calculated by rPBE and PEB functionals with/without D$_3$ correction.

	rPBE	rPBE+ZPE	rPBE+ZPE+D$_3$	PBE[a]	PBE+ZPE	PBE+ZPE+D$_3$
			Ru(0001)			
CO	-1.70	-1.66	-2.00	-1.94	-1.89	-2.23
			Ru(111)			
CO	-1.83	-1.77	-2.06	-2.07	-2.00	-2.40
CH$_4$	0	0.04	-0.05	-0.02 [-0.02]	-0.01	-0.17
CH$_3$CH$_3$	0.01	0.03	-0.15	-0.02[-0.03]	-0.03	-0.36
CH$_3$CH$_2$CH$_3$	0.01	0.04	-0.21	-0.04	-0.06	-0.35
CH$_3$	-1.77	-1.68	-2.11	-2.22[-2.05]	-2.13	-2.67
CH$_3$CH$_2$	-1.35	-1.26	-1.90	-1.83[-1.76]	-1.76	-2.48
CH$_3$CH$_2$CH$_2$	-1.31	-1.27	-2.03	-1.84	-1.77	-2.66

(a)   PBE p(2x2) Ru(0001) results from Ref[1] are given in square bracket.

Table S2. Zero point energy (ZPE) effect on the energy barriers and reaction energies of the minimum energy path of CH$_4$ successive dissociation on the Ru(111) surface. d_{Ru-C} and d_{Ru-H} respectively for the distance between the top layer Ru atoms and the closet C atom and H atom (the values of d_{Ru-C} and d_{Ru-H} greater than 2.5 Å are not listed), $d_{breaking}$ for the length of the breaking bond in transition states.

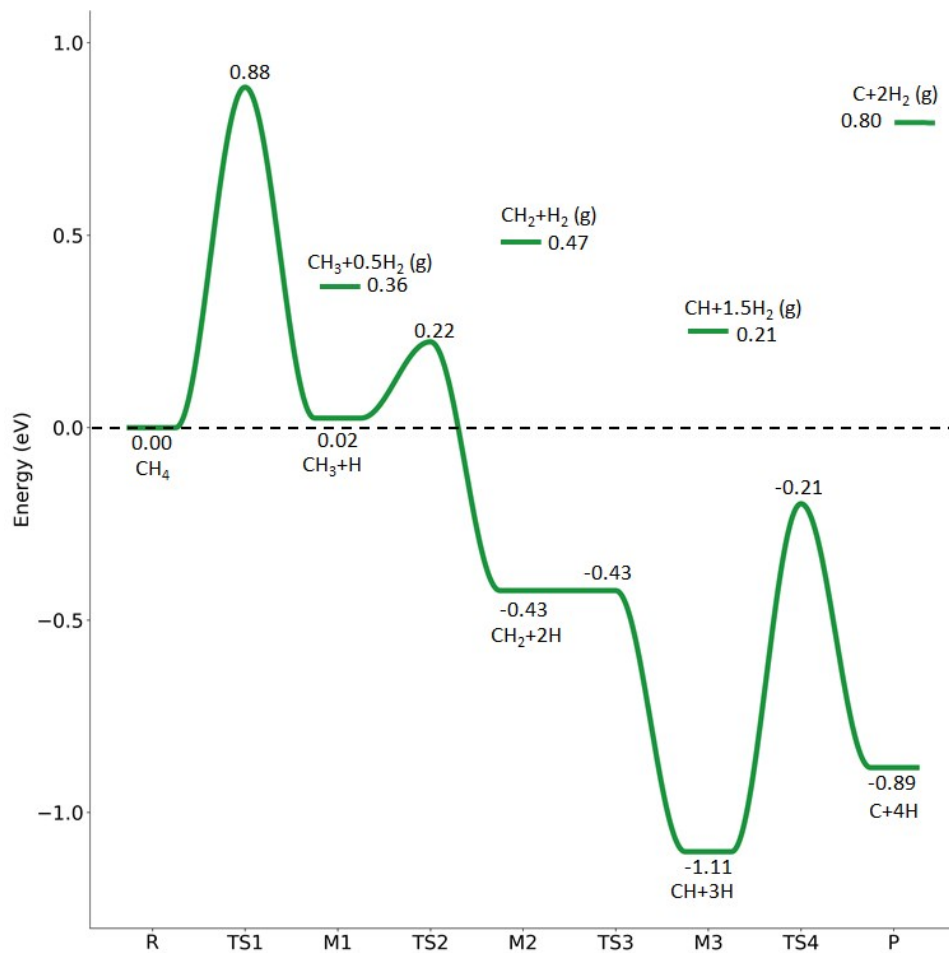| Reactions	E$_a$ (eV)	E$_r$ (eV)	E$_{a (ZPE)}$ (eV)	E$_{r (ZPE)}$ (eV)	E$_{a(G)}$(eV)	ΔG(eV)	d_{Ru-C} (Å)	d_{Ru-H} (Å)	$d_{breaking}$ (Å)
CH$_4$ ⇋ CH$_3$+H	1.03	0.21	0.88	0.02	0.95	0.19	2.284	1.678	1.606
CH$_3$ ⇋ CH$_2$+H	0.33	-0.32	0.20	-0.45	0.23	-0.41	2.102; 2.129; 2.229	1.672	1.571
CH$_2$ ⇋ CH+H	0.07	-0.62	-0.03	-0.68	-0.03	-0.66	2.057; 2.057; 2.062	1.675	1.491
CH ⇋ C+H	1.01	0.30	0.90	0.22	0.93	0.21	1.947; 1.950; 1.974	1.676	1.654

Figure S1. Potential energy surface of CH_4^* consecutive C−H dissociation (energy level on the basis of adsorbed CH_4^*); and the energy level of surface carbonaceous species and gaseous H_2 is also given for comparison.
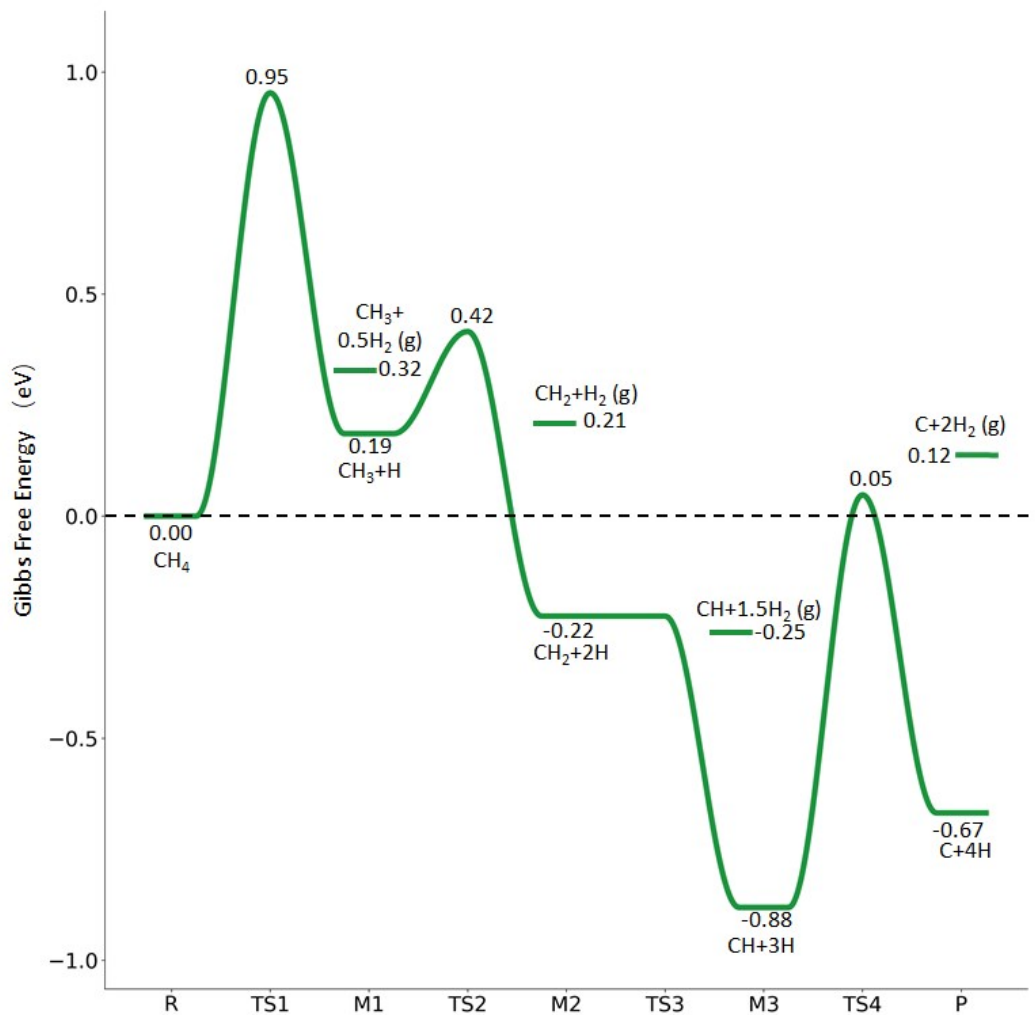
Figure S2. Gibbs free energy profiles of methane dehydrogenation at 490 K and 19.7 atm H_2 (energy level on the basis of adsorbed CH_4^*); and the energy level of surface carbonaceous species and gaseous H_2 is also given for comparison.

Table S3. Zero point energy (ZPE) effect on the energy barriers and reaction energies of elementary reactions of the minimum energy path of CH_3CH_3 successive dissociation on the Ru(111) surface. d_{Ru-C} and d_{Ru-H} respectively for the distance between the top layer Ru atoms and the closet C atom and H atom (the values of d_{Ru-C} and d_{Ru-H} greater than 2.5 Å are not listed), $d_{breaking}$ for the length of the breaking bond in transition states. C_1 and C_2 respectively represent for the two C atoms nearest from the surface.

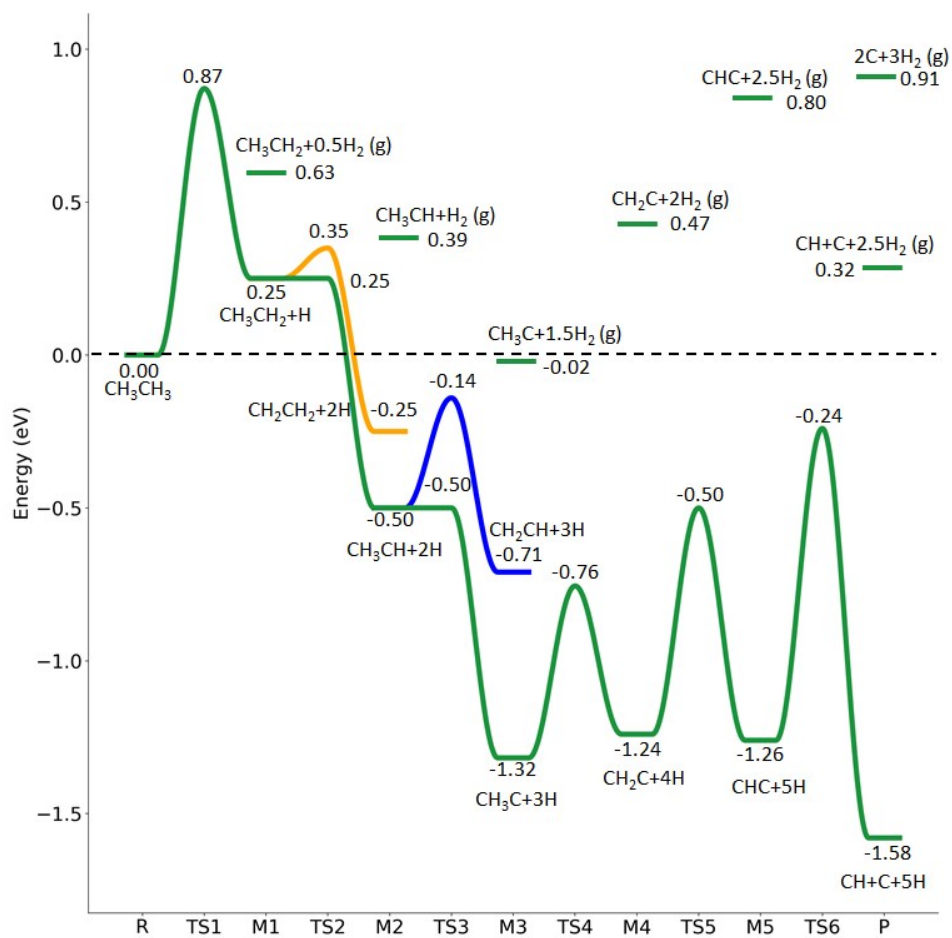| Reactions	E_a (eV)	E_r (eV)	$E_{a\ (ZPE)}$ (eV)	$E_{r\ (ZPE)}$ (eV)	$E_{a(G)}$ (eV)	ΔG (eV)	d_{Ru-C} (Å)	d_{Ru-H} (Å)	$d_{breaking}$ (Å)
$CH_3CH_3 \leftrightarrows CH_3CH_2+H$	1.04	0.48	0.87	0.25	0.89	0.26	2.314	1.656	1.619
$CH_3CH_3 \leftrightarrows CH_3+CH_3$	2.50	0.36	2.28	0.10	2.25	0.09	2.176 (C_1); 2.219 (C_2)		1.894
$CH_3CH_2 \leftrightarrows CH_3CH+H$	0.09	-0.63	0.00	-0.75	0.03	-0.74	2.137; 2.146; 2.270	1.669	1.516
$CH_3CH_2 \leftrightarrows CH_2CH_2+H$	0.19	-0.40	0.10	-0.50	0.13	-0.49	2.224 (C_1); 2.227 (C_1); 2.392(C_2); 2.391(C_2)	1.698	1.529
$CH_3CH_2 \leftrightarrows CH_3+CH_2$	0.86	-0.42	0.78	-0.55	0.77	-0.51	2.074 (C_1); 2.332 (C_2)		2.006
$CH_3CH \leftrightarrows CH_3C+H$	0.01	-0.77	-0.05	-0.82	-0.01	-0.82	2.080; 2.081; 2.101	1.673	1.421
$CH_3CH \leftrightarrows CH_2CH+H$	0.49	-0.04	0.36	-0.21	0.43	-0.02	2.257	1.683	1.585
$CH_3CH \leftrightarrows CH_3+CH$	0.96	-0.36	0.93	-0.45	0.98	-0.41	2.053 (C_1); 2.346 (C_2)		1.932
$CH_3C \leftrightarrows CH_2C+H$	0.69	0.22	0.56	0.08	0.66	0.16	2.292	1.680	1.637
$CH_3C \leftrightarrows CH_3+C$	1.53	0.69	1.44	0.58	1.54	0.64	1.949 (C_1); 2.315 (C_2)		2.113
$CH_2C \leftrightarrows CHC+H$	0.90	0.11	0.74	-0.02	0.74	-0.01	2.199; 2.252	1.728	1.467
$CH_2C \leftrightarrows CH_2+C$	1.66	0.38	1.55	0.28	1.60	0.29	1.982 (C_1); 2.036 (C_2)		2.068
$CHC \leftrightarrows CC+H$	1.49	0.52	1.34	0.42	1.33	0.43	1.986; 2.115; 2.119	1.713	1.611
$CHC \leftrightarrows CH+C$	1.07	-0.28	1.02	-0.32	1.04	-0.30	1.941 (C_1); 2.001 (C_1); 1.938 (C_2);1.947 (C_2);2.011 (C_2)		2.080
$CH+C+H \leftrightarrows 2CH$	0.77	-0.37	0.69	-0.28	0.68	-0.29	1.979	1.670	1.628

Figure S3. Partial potential energy surface of $CH_3CH_3^*$ consecutive dissociation (energy level on the basis of adsorbed $CH_3CH_3^*$); the minimum energy path is in green, the path of $CH_3CH_2^*+H^* \to CH_2^*CH_2^*+2H^*$ is in orange, and the path of $CH_3CH^*+2H^* \to CH_2CH^*+3H^* \to CH_2C^*+4H^*$ is in blue; and the energy level of surface carbonaceous species and gaseous H_2 is also given for comparison.
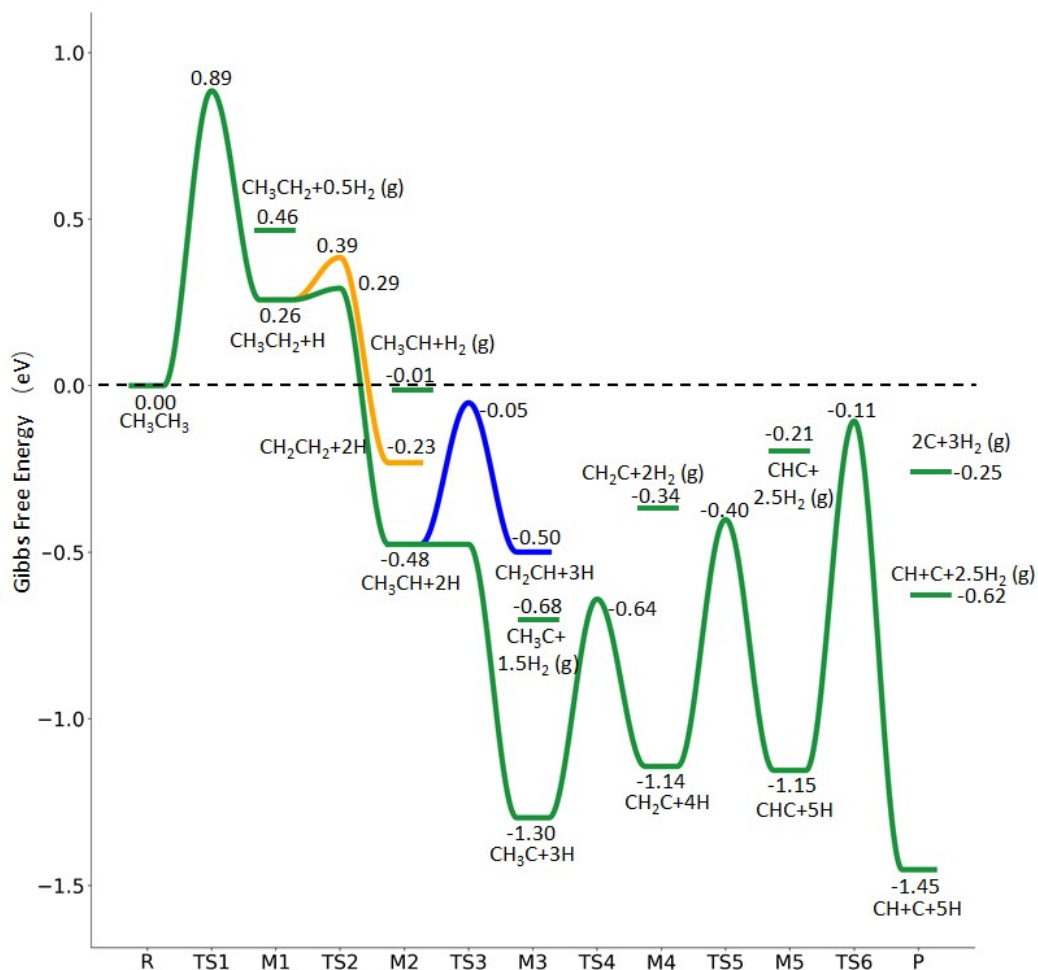
Figure S4. Partial Gibbs free energy profiles of CH_3CH_3* consecutive dissociation at 490 K and 19.7 atm H_2 (energy level on the basis of adsorbed CH_3CH_3*); the minimum energy path is in green, the path of CH_3CH_2*+H* → CH_2*CH_2*+2H* is in orange, and the path of CH_3CH*+2H* → CH_2CH*+3H* → CH_2C*+4H* is in blue; and the energy level of surface carbonaceous species and gaseous H_2 is also given for comparison.

For comparing hcp Ru(0001) and fcc Ru(111) surface, we calculated the dehydrogenation of CH_3CH_2*. In this part, we used a $p(4\times4)$ hcp Ru(0001) slab to make sure the same coverage with fcc Ru(111) surface. The calculated equilibrium lattice constants for the hcp ruthenium phase are $a = b = 2.732$ Å, $c = 4.324$ Å, in agreement with the experiments ($a = b = 2.751$ Å, $c = 4.282$ Å).[2] All calculation methods and accuracy are as the same with fcc Ru(111) surface.

Table S4. A comparison of the barrier(eV) and reaction energies(ev) of CH_3CH_2* dehydrogenation on Ru (111) or Ru (0001) surface, including zero point energy (ZPE) correction. d_{Ru-C} and d_{Ru-H} respectively for the distance between the top layer Ru atoms and the closet C atom and H atom (the values of d_{Ru-C} and d_{Ru-H} greater than 2.5 Å are not listed), $d_{breaking}$ for the length of the breaking bond in transition states. C_1 and C_2 respectively represent for the two C atoms nearest from the surface.

Reactions	Facets	E_a	$E_{a(ZPE)}$	E_r	$E_{r(ZPE)}$	d_{Ru-C} (Å)	d_{Ru-H} (Å)	$d_{breaking}$ (Å)
$CH_3CH_2+H \leftrightarrows CH_2CH_2+2H$	Ru(0001)	0.36	0.24	-0.21	-0.35	2.243 (C_1); 2.231 (C_1); 2.495 (C_2); 2.490 (C_2)	1.720	1.518
	Ru(111)	0.19	0.10	-0.40	-0.50	2.224 (C_1); 2.227 (C_1); 2.392 (C_2); 2.391 (C_2)	1.698	1.529
$CH_3CH_2+H \leftrightarrows CH_3CH+2H$	Ru(0001)	0.36	0.23	-0.20	-0.35	2.161; 2.120; 2.328	1.660	1.618
	Ru(111)	0.09	0.00	-0.63	-0.75	2.137; 2.146; 2.270	1.669	1.516

Table S5. ZPE-corrected adsorption energies (eV) of CH_3CH_2*, CH_2*CH_2*, CH_3CH* and $H*$ on $p(4\times4)$ Ru(0001) surface, d_{c-c} for the length of the nearest C-C bond from surface, d_{Ru-C} and d_{Ru-H} respectively for the distance between the top layer Ru atoms and the closet C atom and H atom (the values of d_{Ru-C} and d_{Ru-H} greater than 2.5 å are not listed), d_{C-H} for the length of the longest C-H bond in adsorbed C atoms, as well as f for fcc, h for hcp, b for $bridge$ and t for top sites.

	Site	E_{ads}	d_{C-C} (Å)	d_{Ru-C} (Å)	d_{Ru-H} (Å)	d_{C-H} (Å)
CH_3CH_2	h	-1.23	1.546	2.208; 2.468; 2.486	2.064; 2.039	1.140; 1.145
CH_2CH_2	$h+t$	-0.56	1.451	2.169 (t); 2.248 (f); 2.477 (f); 2.493(f)	2.165; 2.186	1.119
CH_3CH	h	-3.43	1.522	2.101; 2.267;2.100	1.822	1.206
H	f	-2.78			1.908; 1.912; 1.930	

Table S6. Zero point energy (ZPE) effect on the energy barriers and reaction energies of elementary reactions of CH_3CH_3 successive dissociation on the Ru(111) surface except the minimum energy path. d_{Ru-C} and d_{Ru-H} respectively for the distance between the top layer Ru atoms and the closet C atom and H atom (the values of d_{Ru-C} and d_{Ru-H} greater than 2.5 Å are not listed), $d_{breeking}$ for the length of the breaking bond in transition states. C_1 and C_2 respectively represent for the two C atoms nearest from the surface.

Reactions	E_a (eV)	E_r (eV)	$E_{a\,(ZPE)}$ (eV)	$E_{r\,(ZPE)}$ (eV)	$E_{a(G)}$ (eV)	ΔG (eV)	d_{Ru-C} (Å)	d_{Ru-H} (Å)	$d_{breeking}$ (Å)
$CH_2CH_2 \leftrightarrows CH_2CH+H$	0.26	-0.26	0.13	-0.46	0.20	-0.34	2.083; 2.166; 2.264	1.680	1.551
$CH_2CH_2 \leftrightarrows CH_2+CH_2$	1.27	-0.19	1.15	-0.37	1.20	-0.29	2.057 (C_1); 2.060 (C_2)		2.018
$CH_2CH \leftrightarrows CH_2C+H$	0.11	-0.51	0.05	-0.53	0.05	-0.57	2.048; 2.050; 2.103	1.682	1.504
$CH_2CH \leftrightarrows CHCH+H$	0.30	-0.53	0.27	-0.57	0.24	-0.61	2.105; 2.214	1.675	1.520
$CH_2CH \leftrightarrows CH_2+CH$	0.97	-0.47	0.96	-0.52	0.88	-0.55	1.968 (C_1); 2.088 (C_2)		2.032
$CHCH \leftrightarrows CHC+H$	0.75	0.12	0.62	0.02	0.63	0.03	1.958; 2.062; 2.064	1.698	1.602
$CHCH \leftrightarrows CH+CH$	0.89	-0.52	0.83	-0.58	0.86	-0.56	1.975 (C_1);2.031 (C_1); 1.978 (C_2),2.030 (C_2)		1.922
$CC \leftrightarrows C+C$	1.57	-0.39	1.51	-0.39	1.50	-0.38	1.856 (C_1),1.923 (C_1); 1.898 (C_2),1.917 (C_2),2.165 (C_2)		2.255

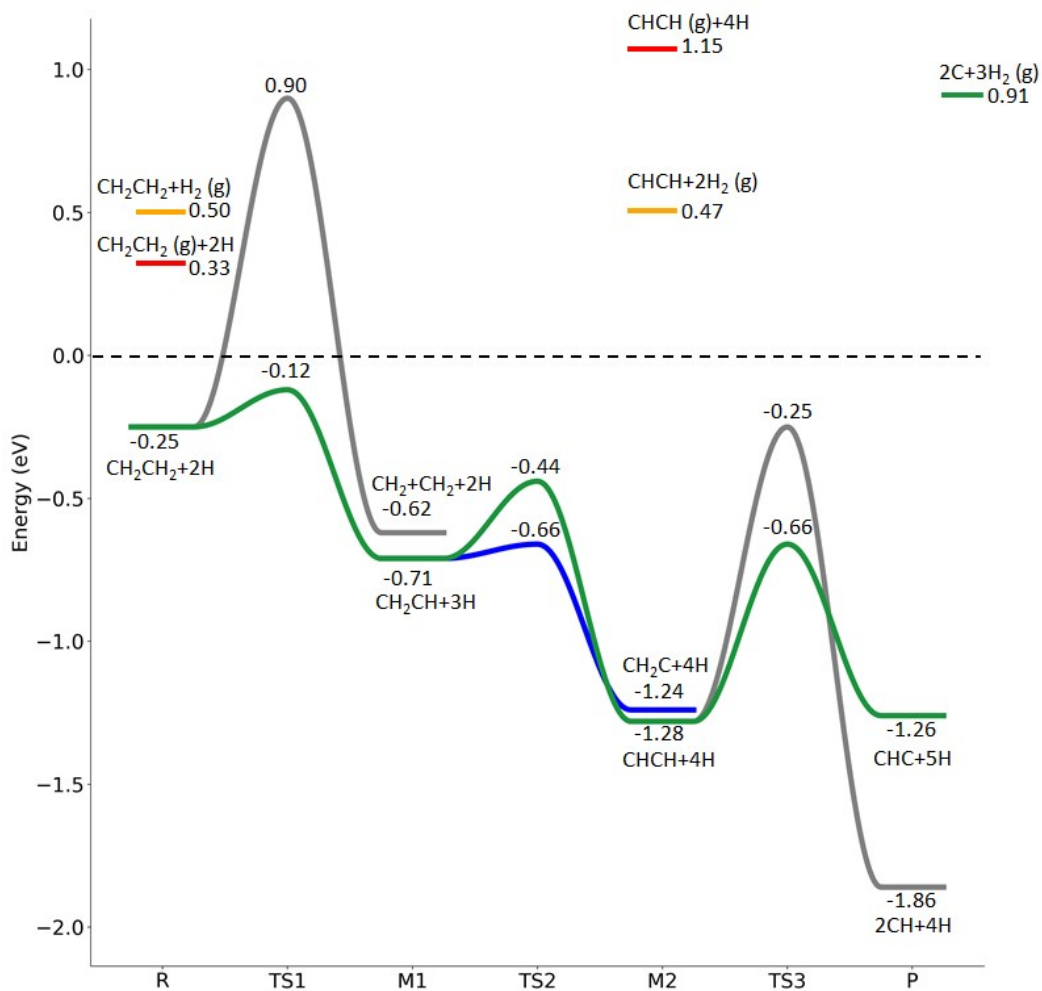**Figure S5.** Potential energy surface of CH_2*CH_2* consecutive dissociation (energy level on the basis of adsorbed CH_3CH_3*); combined with Figure S3, a complete potential energy surface of CH_3CH_3* dissociation is presented; the path of ethene dissociation through ethyne intermediate is in green; the desorption of molecularly adsorbed CH_2*CH_2* and $CH*CH*$, surface $H*$ and the break of C-C bond for CH_2*CH_2*+2H* and $CH*CH*+4H*$ are given in red, orange, and grey, respectively.
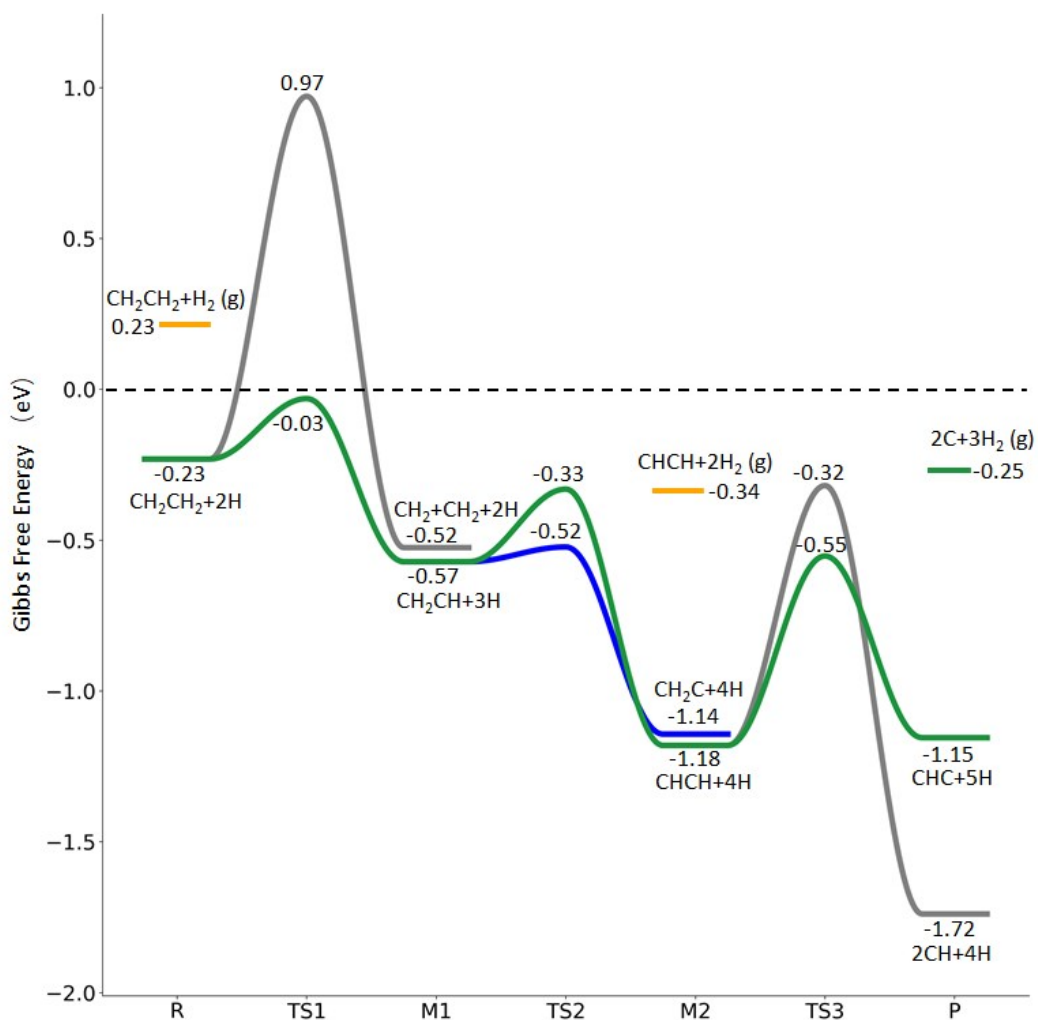
Figure S6. Gibbs free energy profiles of CH_2*CH_2* consecutive dissociation at 490 K and 19.7 atm H_2 (energy level on the basis of adsorbed CH_3CH_3*); combined with Figure S4, a complete potential energy surface of CH_3CH_3* dissociation is presented; the path of ethene dissociation through ethyne intermediate is in green; the desorption of surface H* and the break of C-C bond for CH_2*CH_2*+2H* and $CH*CH*+4H*$ are given in orange, and grey, respectively.

Table S7. Zero point energy (ZPE) effect on the energy barriers and reaction energies of elementary reactions of the minimum energy path of $CH_3CH_2CH_3$ successive dissociation on the Ru(111) surface. d_{Ru-C} and d_{Ru-H} respectively for the distance between the top layer Ru atoms and the closet C atom and H atom (the values of d_{Ru-C} and d_{Ru-H} greater than 2.5 Å are not listed), $d_{breaking}$ for the length of the breaking bond in transition states. C_1 and C_2 respectively represent for the two C atoms nearest from the surface.

Reactions	E_a(eV)	E_r(eV)	$E_{a\,(ZPE)}$(eV)	$E_{r\,(ZPE)}$(eV)	$E_{a(G)}$(eV)	ΔG(eV)	d_{Ru-C}(Å)	d_{Ru-H}(Å)	$d_{breaking}$(Å)
$CH_3CH_2CH_3 \leftrightarrows CH_3CH_2CH_2+H$	1.11	0.45	0.93	0.25	0.79	0.15	2.323	1.684	1.642
$CH_3CH_2CH_3 \leftrightarrows CH_3CHCH_3+H$	1.07	0.61	0.89	0.47	0.76	0.40	2.356	1.664	1.672
$CH_3CH_2CH_3 \leftrightarrows CH_3CH_2+CH_3$	2.88	0.81	2.67	0.56	2.53	0.39	2.174 (C_1); 2.261 (C_2)		1.947
$CH_3CH_2CH_2 \leftrightarrows CH_3CH_2CH+H$	0.28	-0.54	0.13	-0.70	0.15	-0.65	2.118; 2.156; 2.271	1.671	1.568
$CH_3CH_2CH_2 \leftrightarrows CH_2CHCH_2+H$	0.25	-0.39	0.13	-0.51	0.16	-0.53	2.202; 2.269	1.701	1.522
$CH_3CH_2CH_2 \leftrightarrows CH_3CH_2+CH_2$	0.95	0.04	0.85	-0.14	0.83	-0.19	2.070 (C_1); 2.383 (C_2)		2.046
$CH_3CH_2CH \leftrightarrows CH_3CH_2C+H$	0.02	-0.79	-0.01	-0.83	-0.11	-0.89	2.083; 2.093; 2.130	1.673	1.406
$CH_3CH_2CH \leftrightarrows CH_2CHCH+H$	0.47	-0.10	0.34	-0.22	0.28	-0.26	2.308	1.683	1.590
$CH_3CH_2CH \leftrightarrows CH_3CH_2+CH$	0.96	-0.06	0.93	-0.13	0.86	-0.18	2.043 (C_1); 2.388 (C_2)		1.987
$CH_3CH_2C \leftrightarrows CH_3CHC+H$	0.66	0.11	0.51	-0.04	0.55	-0.01	2.354	1.680	1.686
$CH_3CH_2C \leftrightarrows CH_3CH_2+C$	1.71	0.99	1.61	0.87	1.71	0.88	1.936 (C_1); 2.374 (C_2)		2.147
$CH_3CHC \leftrightarrows CH_3CC+H$	0.89	0.05	0.89	-0.09	0.78	-0.09	2.250; 2.278	1.737	1.483
$CH_3CHC \leftrightarrows CH_3CH+C$	1.79	0.43	1.70	0.32	1.78	0.33	1.987 (C_1); 2.042 (C_2)		2.304
$CH_3CC \leftrightarrows CH_3C+C$	1.04	-0.31	0.99	-0.34	0.99	-0.33	1.955 (C_1); 2.040 (C_1); 1.946 (C_2); 1.950 (C_2); 1.998 (C_2)		2.059
$CH_3CC \leftrightarrows CH_3+CC$	2.00	1.28	1.96	1.20	2.08	1.27	1.955 (C_1); 2.094 (C_1); 2.139 (C_1); 2.358 (C_2)		2.153
$CH_3C+C+H \leftrightarrows CH_3C+CH$	0.77	-0.35	0.68	-0.29	0.64	0.41	1.974	1.671	1.630

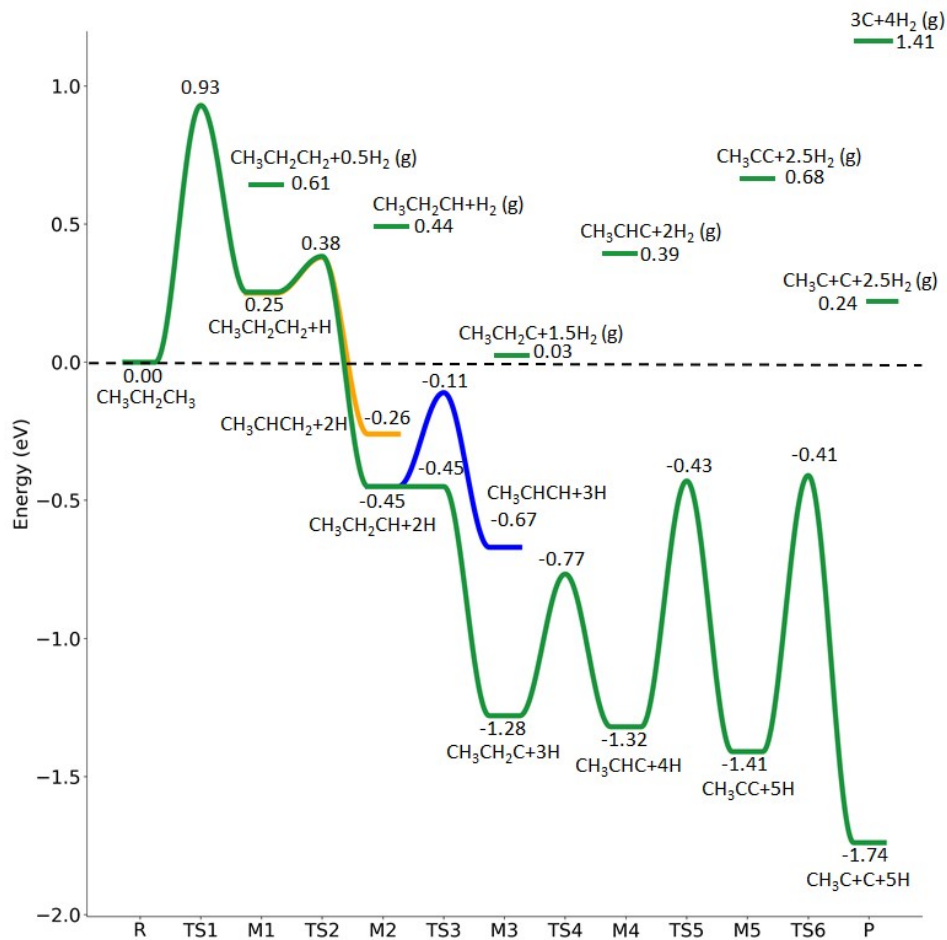**Figure S7.** Partial potential energy surface of $CH_3CH_2CH_3^*$ consecutive dissociation (energy level on the basis of adsorbed $CH_3CH_2CH_3^*$); the minimum energy path is in green, the path of $CH_3CH_2CH_2^*+H^* \rightarrow CH_3CH^*CH_2^*+2H^*$ is in orange, and the path of $CH_3CH_2CH^*+2H^* \rightarrow CH_3CH^*CH^*+3H^* \rightarrow CH_3CH^*C^*+4H^*$ is in blue; and the energy level of surface carbonaceous species and gaseous H_2 is also given for comparison.

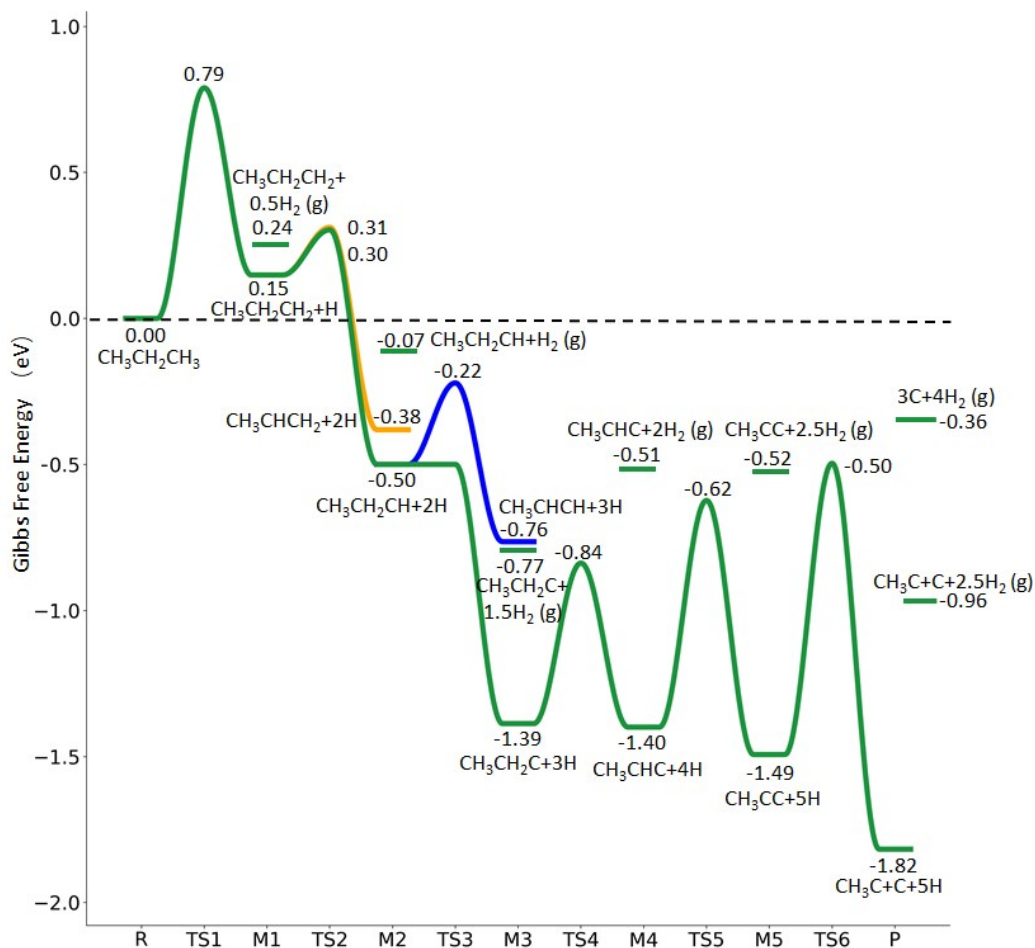**Figure S8.** Gibbs free energy profiles of $CH_3CH_2CH_3^*$ consecutive dissociation at 490 K and 19.7 atm H_2 (energy level on the basis of adsorbed $CH_3CH_2CH_3^*$); the minimum energy path is in green, the path of $CH_3CH_2CH_2^*+H^* \rightarrow CH_3CH^*CH_2^*+2H^*$ is in orange, and the path of $CH_3CH_2CH^*+2H^* \rightarrow CH_3CH^*CH^*+3H^* \rightarrow CH_3CH^*C^*+4H^*$ is in blue; and the energy level of surface carbonaceous species and gaseous H_2 is also given for comparison.

Table S8. Zero point energy (ZPE) effect on the energy barriers and reaction energies of elementary reactions of $CH_3CH_2CH_3$ successive dissociation on the Ru(111) surface except the minimum energy path. d_{Ru-C} and d_{Ru-H} respectively for the distance between the top layer Ru atoms and the closet C atom and H atom (the values of d_{Ru-C} and d_{Ru-H} greater than 2.5 Å are not listed), $d_{breaking}$ for the length of the breaking bond in transition states. C_1 and C_2 respectively represent for the two C atoms nearest from the surface.

Reactions	E_a (eV)	E_r (eV)	$E_{a\,(ZPE)}$ (eV)	$E_{r\,(ZPE)}$ (eV)	$E_{a(G)}$ (eV)	ΔG (eV)	d_{Ru-C} (Å)	d_{Ru-H} (Å)	$d_{breaking}$ (Å)
$CH_3CHCH_3 \leftrightharpoons CH_3CHCH_2+H$	0.93	-0.10	0.73	-0.73	0.71	0.78		1.716	1.581
$CH_3CHCH_3 \leftrightharpoons CH_3CCH_3+H$	0.57	-0.28	0.37	-0.46	0.33	-0.55	1.999	1.680	1.660
$CH_3CHCH_3 \leftrightharpoons CH_3CH+CH_3$	1.27	-0.46	1.16	-0.69	1.05	-0.80	2.082 (C_1); 2.333 (C_1); 2.310 (C_2)		2.013
$CH_3CHCH_2 \leftrightharpoons CH_3CHCH+H$	0.41	-0.25	0.24	-0.41	0.28	-0.38	2.101; 2.128; 2.244	1.688	1.579
$CH_3CHCH_2 \leftrightharpoons CH_3CCH_2+H$	0.33	-0.12	0.18	-0.32	0.23	-0.26	2.090; 2.281	1.672	1.548
$CH_3CHCH_2 \leftrightharpoons CH_3CH+CH_2$	1.17	-0.11	1.04	-0.30	0.90	-0.24	2.003 (C_1); 2.120 (C_2)		2.100
$CH_3CCH_3 \leftrightharpoons CH_3CCH_2+H$	0.50	-0.38	0.34	-0.57	0.36	-0.49	2.273	1.646	1.560
$CH_3CCH_3 \leftrightharpoons CH_3C+CH_3$	0.81	-0.96	0.76	-1.06	0.85	-1.06	2.179 (C_1); 2.306 (C_2)		1.985
$CH_3CHCH \leftrightharpoons CH_3CHC+H$	0.10	-0.59	0.03	-0.65	0.03	-0.64	2.051; 2.069; 2.099	1.673	1.524
$CH_3CHCH \leftrightharpoons CH_3CCH+H$	0.24	-0.56	0.15	-0.66	0.17	-0.64	2.134; 2.270	1.676	1.481
$CH_3CHCH \leftrightharpoons CH_3CH+CH$	0.88	-0.46	0.84	-0.54	0.95	-0.51	1.973 (C_1); 2.108 (C_2)		2.055
$CH_3CCH_2 \leftrightharpoons CH_3CCH+H$	0.18	-0.69	0.09	-0.75	0.08	-0.76	2.109; 2.207	1.672	1.528
$CH_3CCH_2 \leftrightharpoons CH_3C+CH_2$	1.08	-0.75	1.04	-0.79	0.99	-0.81	1.951 (C_1); 2.189 (C_2)		2.016
$CH_3CCH \leftrightharpoons CH_3CC+H$	0.72	0.03	0.58	-0.10	0.54	-0.09	1.966; 2.061; 2.073	1.699	1.601
$CH_3CCH \leftrightharpoons CH_3C+CH$	1.04	-0.63	0.85	-0.71	0.80	-0.68	1.991 (C_1); 2.051 (C_1); 2.313 (C_1); 1.986 (C_2); 2.035 (C_2)		1.922

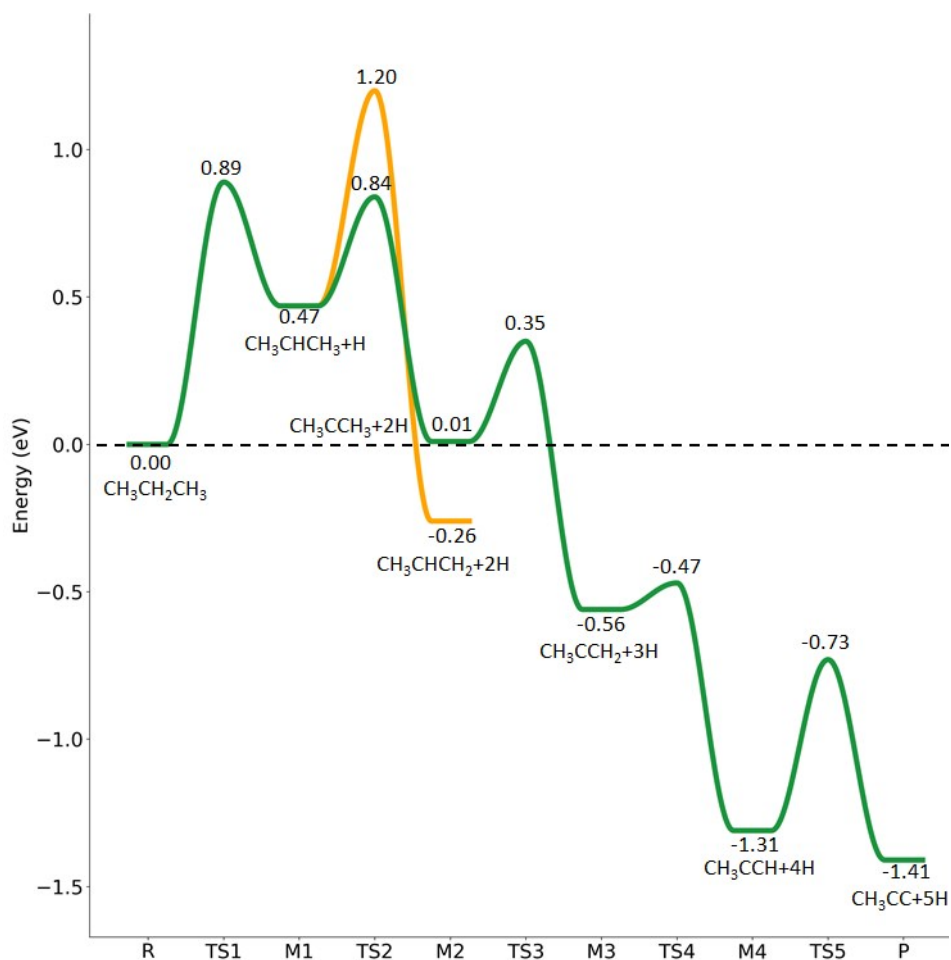**Figure S9.** Partial supplement to potential energy surface of $CH_3CH_2CH_3$* consecutive dissociation adsorption (energy level on the basis of adsorbed $CH_3CH_2CH_3$*); the path of $CH_3CH^*CH_3+H^* \rightarrow CH_3CCH_3^*+2H^* \rightarrow CH_3C^*CH_2^*+3H^* \rightarrow CH_3C^*CH^*+4H8 \rightarrow CH_3C^*C^*+5H^*$ is in green, the path of $CH_3CH^*CH_3+H^* \rightarrow CH_3CH^*CH_2^*+2H^*$ is in orange.
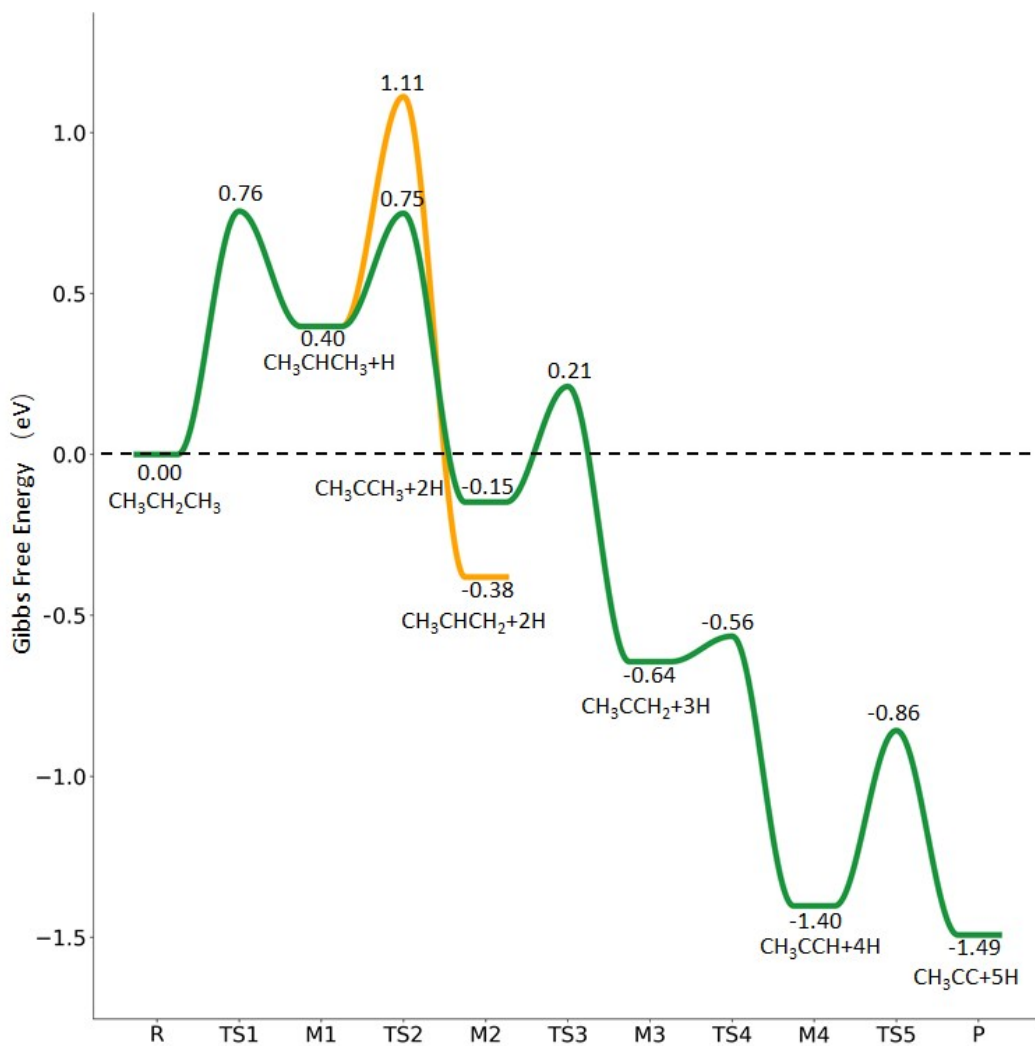
Figure S10. Partial supplement to Gibbs free energy profiles of $CH_3CH_2CH_3*$ consecutive dissociation adsorption at 490 K and 19.7 atm H_2 (energy level on the basis of adsorbed $CH_3CH_2CH_3*$); the path of $CH_3CH*CH_3+H* \rightarrow CH_3CCH_3*+2H* \rightarrow CH_3C*CH_2*+3H* \rightarrow CH_3C*CH*+4H8 \rightarrow CH_3C*C*+5H*$ is in green, the path of $CH_3CH*CH_3+H* \rightarrow CH_3CH*CH_2*+2H*$ is in orange.
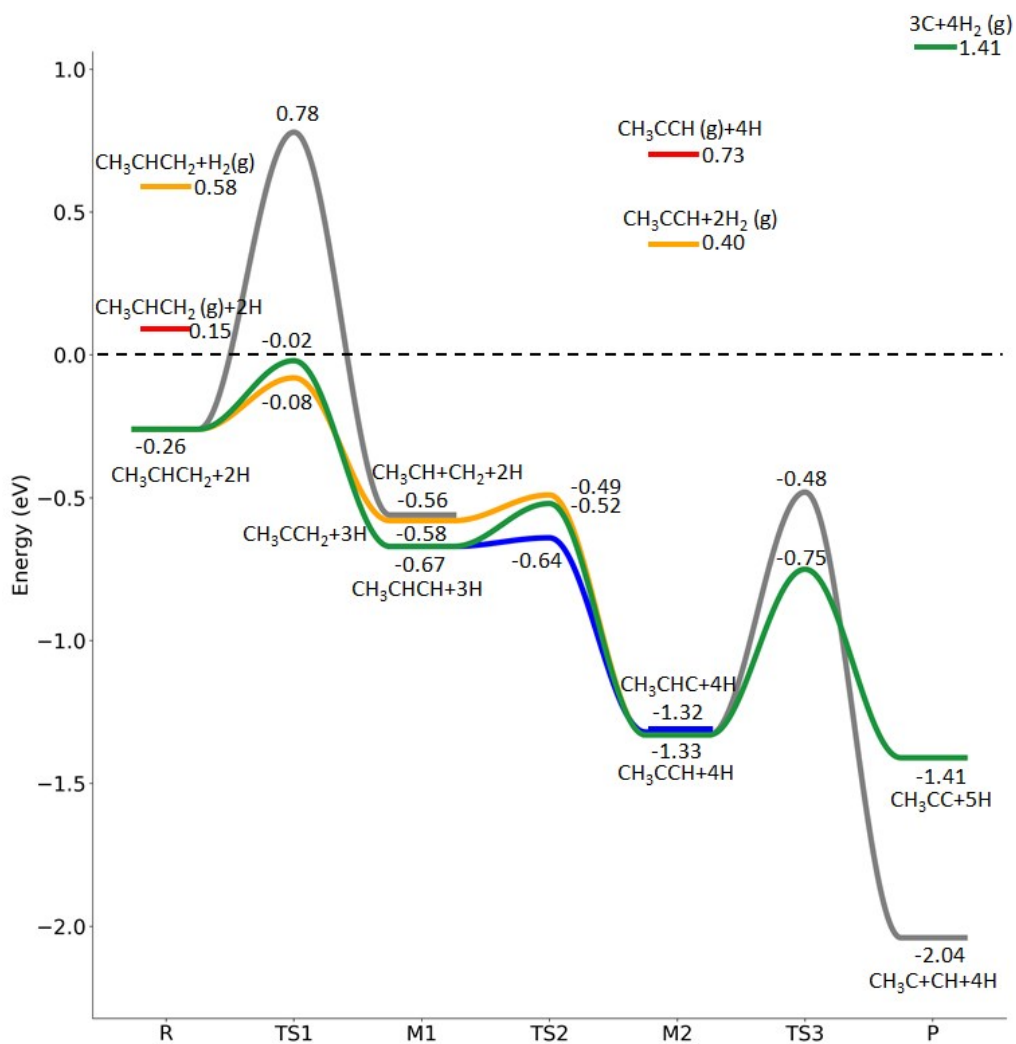
Figure S11. Potential energy surface of CH_3CH*CH_2* consecutive dissociation (energy level on the basis of adsorbed $CH_3CH_2CH_3*$); combined with Figures S7 and S9, a complete potential energy surface of $CH_3CH_2CH_3*$ dissociation is presented; the path of propene dissociation through propyne intermediate is in green; the path of $CH_3CH*CH_2*+2H* \rightarrow CH_3C*CH_2*+3H* \rightarrow CH_3C*CH*+4H*$ is in orange; the path of $CH_3CH*CH*+3H* \rightarrow CH_3CH*C*+4H*$ is in blue; the desorption of molecularly adsorbed CH_3CH*CH_2* and CH_3C*CH*, surface $H*$ and the break of C-C bond for CH_3CH*CH_2*+2H* and $CH_3C*CH*+4H*$ are respectively in red, orange, and grey.
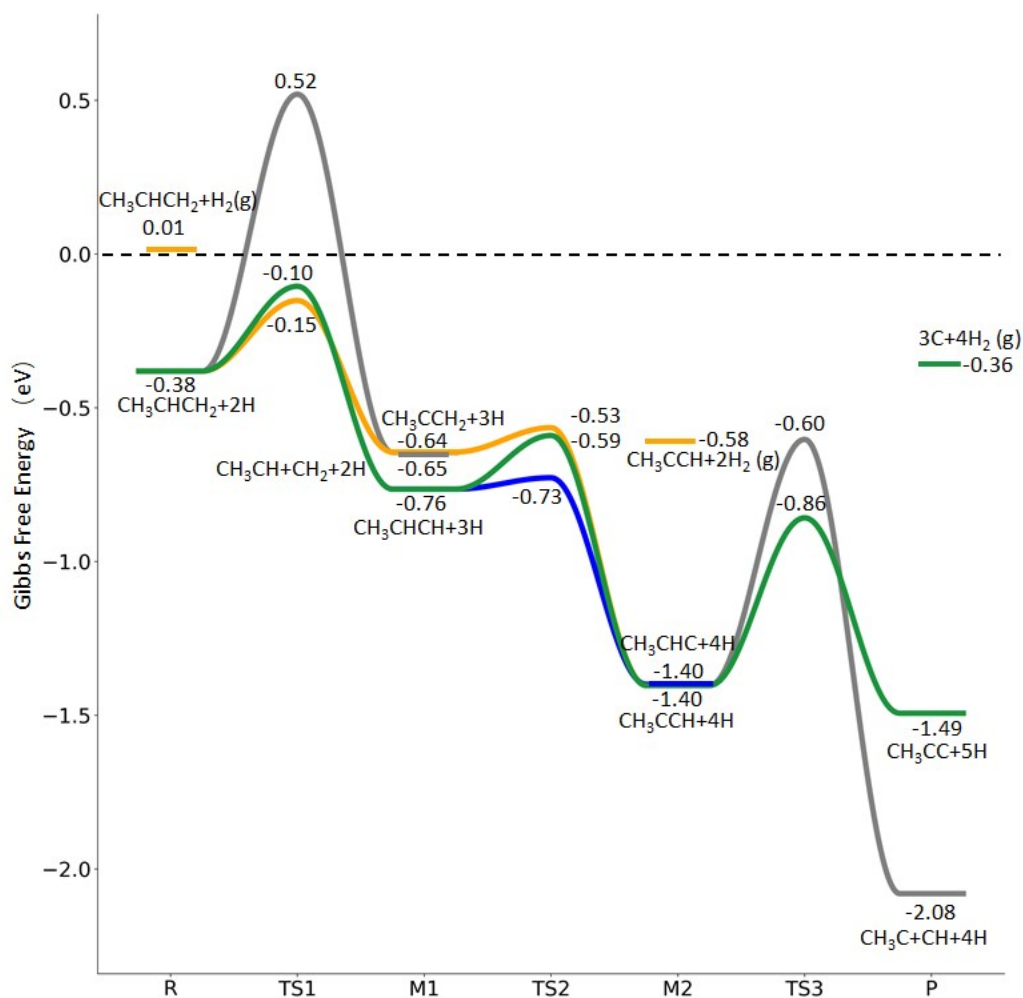
Figure S12. Gibbs free energy profiles of CH_3CH*CH_2* consecutive dissociation at 490 K and 19.7 atm H_2 (energy level on the basis of adsorbed $CH_3CH_2CH_3*$); combined with Figures S8 and S10, a complete potential energy surface of $CH_3CH_2CH_3*$ dissociation is presented; the path of propene dissociation through propyne intermediate is in green; the path of $CH_3CH*CH_2*+2H* \rightarrow CH_3C*CH_2*+3H* \rightarrow CH_3C*CH*+4H*$ is in orange; the path of $CH_3CH*CH*+3H* \rightarrow CH_3CH*C*+4H*$ is in blue; the desorption of surface H* and the break of C-C bond for CH_3CH*CH_2*+2H* and $CH_3C*CH*+4H*$ are respectively in orange and grey

Table S9. Computed vibrational frequencies of CH$_3$*, CH$_3$CH$_2$*, and CH$_3$CH$_2$CH$_2$* adsorbed on the Ru(111) surface. (ν, δ, ρ, ω, and τ represent the mode of stretching, scissoring, rocking, wagging and twisting, respectively, the subscript of a and s represent the asymmetric and symmetric modes, respectively.)

CH$_3$*	Mode	CH$_3$CH$_2$*	Mode	CH$_3$CH$_2$CH$_2$*	Mode
2862	ν$_s$(CH$_3$)	3074	ν$_a$(CH$_3$)	3073	ν$_s$(CH$_3$) ν$_s$ (centre CH$_2$)
2824	ν(CH$_3$)	3062	ν$_s$(CH$_3$)	3055	ν$_a$ (CH$_3$) ν (centre CH$_2$)
2811	ν(CH$_3$)	2977	ν(CH$_3$)	3047	ν(CH$_3$)
1309	δ$_a$(CH$_3$)	2465	ν(CH$_3$)	3033	ν(CH$_3$) ν(centre CH$_2$)
1303	δ$_a$(CH$_3$)	2422	ν(CH$_3$)	2978	ν(centre CH$_2$)
1178	δ$_s$(CH$_3$)	1457	δ$_a$(CH$_3$)	2375	ν$_s$(end CH$_2$)
		1454	δ$_a$(CH$_3$)	2350	ν$_a$(centre CH$_2$)
		1369	δ$_s$(CH$_3$)	1468	δ$_a$(CH$_3$)
		1356	ω(CH$_2$)	1455	δ$_a$(CH$_3$)
		1319		1446	δ(centre CH$_2$)
		1197	δ(CH$_2$)	1388	
		993		1378	
		983		1371	δ$_s$(CH$_3$)
		943	ν(CC)	1290	ω(centre CH$_2$)
		632	ρ(CH$_2$)	1244	
				1160	δ(end CH$_2$)
				1048	
				1043	ν(far CC)
				1029	ν$_a$(both CC)
				853	ν$_s$(both CC)
				780	

Table S10. Computed vibrational frequencies of CH_2*, CH_3CH* and CH_3CH_2CH* adsorbed on the Ru(111) surface. (v, δ, ρ, ω, and τ represent the mode of stretching, scissoring, rocking, wagging and twisting, respectively, the subscript of a and s represent the asymmetric and symmetric modes, respectively.)

CH_2*	Mode	CH_3CH*	Mode	CH_3CH_2CH*	Mode
2982	$v(CH_2)$	3062	$v(CH_3)$	3075	$v_s(CH_3)$
					$v_s(CH_2)$
1938	$v(CH_2)$	3016	$v(CH_3)$	3051	$v_a(CH_3)$
	$v(Metal\text{-}H)$				
1535	$\delta(CH_2)$	2996	$v(CH_3)$	3037	$v(CH_3)$
696	$\omega(CH_2)$	1808	$v(CH)$	3017	$v_s(CH_2)$
			$v(Metal\text{-}H)$		
678	$\rho(CH_2)$	1490	$v(CH)$	2980	$v_a(CH_2)$
		1430	$\delta_a(CH_3)$	1880	$v(CH)$
					$v(Metal\text{-}H)$
		1427	$\delta_a(CH_3)$	1458	$\delta_a(CH_3)$
		1340	$\delta_s(CH_3)$	1451	$\delta_a(CH_3)$
		980		1425	$\delta(CH_2)$
		961		1371	$\delta_s(CH_3)$
		948	$v(CC)$	1303	
				1269	
				1237	
				1057	$v_a(both\ CC)$
				1048	
				1040	
				878	$v_s(both\ CC)$
				771	

Table S11. Computed vibrational frequencies of CH_3CH*CH_3 and CH_3C*CH_3 adsorbed on the Ru(111) surface. (v, δ, ρ, ω, and τ represent the mode of stretching, scissoring, rocking, wagging and twisting, respectively, the subscript of a and s represent the asymmetric and symmetric modes, respectively.)

CH_3CH*CH_3	Mode	CH_3C*CH_3	Mode
3049	v(1st CH_3)	3010	v(1st CH_3)
3007	v(2nd CH_3)	3007	v_s(2nd CH_3)
			v(1st CH_3)
2990	v(1st CH_3)	3001	v(1st CH_3)
2972	v(2nd CH_3)	2987	v_a(2nd CH_3)
2957	v(1st CH_3)	2939	v(2nd CH_3)
	v(2nd CH_3)		
2952	v_a(2nd CH_3)	2613	v(1st CH_3)
	v(1st CH_3)		
2931	v(CH)	1513	δ_a(1st CH_3)
1454	δ_a(both CH_3)	1435	δ_a(2nd CH_3)
1441	δ_a(both CH_3)	1393	δ_a(2nd CH_3)
1439	δ_a(both CH_3)	1386	δ_s(both CH_3)
1416	δ_a(both CH_3)	1359	δ_s(2nd CH_3)
1369	δ_s(both CH_3)	1319	δ_a(1st CH_3)
1350		1115	
1277		1056	v_a(both CC)
1153		973	
1081		940	v_a(both CC)
1076	v_a(both CC)	926	
933		871	v_s(both CC)
900			
880			
853	v_s(both CC)		

Table S12. Computed vibrational frequencies of $CH*$, CH_3C* and CH_3CH_2C* adsorbed on the Ru(111) surface. (v, δ, ρ, ω, and τ represent the mode of stretching, scissoring, rocking, wagging and twisting, respectively, the subscript of a and s represent the asymmetric and symmetric modes, respectively.)

$HC*$	Mode	CH_3C*	Mode	CH_3CH_2C*	Mode
2985	v(CH)	3039	v(CH_3)	3084	v(CH_3)
709	δ(CH)	3013	v(CH_3)	3055	v_a(CH_3)
672	δ(CH)	2978	v(CH_3)	3031	v_s(CH_3)
					v(CH_2)
		1432	δ_a(CH_3)	3009	v_s(CH_2)
		1427	δ_a(CH_3)	2990	v_a(CH_2)
		1324	Δ_s(CH_3)	1467	δ_a(CH_3)
		1036	v(CC)	1460	δ_a(CH_3)
		971		1424	δ(CH_2)
		967		1370	δ_s(CH_3)
				1277	
				1241	
				1059	v(near CC)
				1037	
				1035	v(far CC)
				917	v_s(both CC)
				769	

Table S13. Computed vibrational frequencies of CH_2*CH_2* and CH_3CH*CH_2* adsorbed on the Ru(111) surface. (ν, δ, ρ, ω, and τ represent the mode of stretching, scissoring, rocking, wagging and twisting, respectively, the subscript of a and s represent the asymmetric and symmetric modes, respectively.)

CH_2*CH_2*	Mode	CH_3CH*CH_2*	Mode
3141	ν_a(far CH_2)	3097	ν_s(CH_3)
			ν(CH)
3094	ν_s(far CH_2)	3087	ν(CH_3)
2815	ν_a(near CH_2)	3042	ν_a(CH_3)
			ν(CH)
2796	ν_s(near CH_2)	2972	ν(CH_3)
1433	δ(far CH_2)	2777	ν(CH_2)
	ν(CC)		
1311	δ(near CH_2)	2675	ν(CH_2)
	ν(CC)		
1179		1455	δ_a(CH_3)
1109	ν(CC)	1439	δ_a(CH_3)
1030	ω(near CH_2)	1373	δ_s(CH_3)
	ν(Metal-C)		
903	ω(far CH_2)	1350	
	ν(CC)		
898		1290	
752		1171	
666	ρ(both CH_2) group	1148	ν_a(both CC)
		1079	
		1020	
		990	
		894	ν_s(both CC)
		841	
		731	

Table S14. Computed vibrational frequencies of CH_2*CH*, $CH_3CH*CH*$, and CH_3C*CH_2* adsorbed on the Ru(111) surface. (ν, δ, ρ, ω, and τ represent the mode of stretching, scissoring, rocking, wagging and twisting, respectively, the subscript of a and s represent the asymmetric and symmetric modes, respectively.)

CH_2*CH*	Mode	$CH_3CH*CH*$	Mode	CH_3C*CH_2*	Mode
3125	$\nu_a(CH_2)$	3100	ν(centre CH)	3034	$\nu(CH_3)$ $\nu(CH_2)$
3084	$\nu_s(CH_2)$	3059	$\nu(CH_3)$	3034	$\nu_s(CH_3)$ $\nu(CH_2)$
2100	ν(CH) ν(Metal-H)	3029	$\nu(CH_3)$	3015	$\nu_a(CH_3)$
1424	$\delta(CH_2)$	2985	$\nu(CH_3)$	2984	$\nu(CH_3)$
1304		2067	ν(end CH) ν(Metal-H)	2297	$\nu(CH_2)$
1179	ν(CC)	1456	$\delta_a(CH_3)$	1456	$\delta(CH_2)$
978		1441	$\delta_a(CH_3)$	1438	$\delta_a(CH_3)$
888	$\omega(CH_2)$	1368	$\delta_s(CH_3)$	1421	$\delta_a(CH_3)$
718		1351		1361	$\delta_a(CH_3)$
652		1325		1214	ν(near CC)
		1198	ν(near CC)	1104	
		1054		1023	
		1010		980	
		925	ν(far CC)	908	ν_s(both CC)
		783		844	
		723		732	$\rho(CH_2)$

Table S15. Computed vibrational frequencies of CH_3C* and CH_3CHC*, $HC*C*$ and CH_3C*C* adsorbed on the Ru(111) surface. (ν, δ, ρ, ω, and τ represent the mode of stretching, scissoring, rocking, wagging and twisting, respectively, the subscript of a and s represent the asymmetric and symmetric modes, respectively.)

CH_2C*	Mode	CH_3CHC*	Mode	$HC*C*$	Mode	CH_3C*C*	Mode
3130	$\nu_a(CH_2)$	3072	$\nu(CH_3)$ ν(CH)	3102	ν(CH)	3091	$\nu_s(CH_3)$
3071	$\nu_s(CH_2)$	3068	$\nu_s(CH_3)$ ν(CH)	1207	ν(CC)	3071	$\nu_a(CH_3)$
1417	$\delta(CH_2)$	3048	$\nu(CH_3)$ ν(CH)	913		3024	$\nu_s(CH_3)$
1247	ν(CC)	2988	$\nu(CH_3)$	753	δ(CH)	1445	$\delta_a(CH_3)$
973	$\rho(CH_2)$	1452	$\delta_a(CH_3)$			1435	$\delta_a(CH_3)$
869	$\omega(CH_2)$	1440	$\delta_a(CH_3)$			1361	$\delta_s(CH_3)$
632	$\tau(CH_2)$	1367	$\delta_s(CH_3)$ ν(near CC)			1323	ν_a(both CC)
		1352	ν_a(both CC)			1030	
		1231	ν(near CC)			973	
		1059				912	ν_s(both CC)
		1016					
		915	ν(far CC)				
		794					

Table S16. Computed vibrational frequencies of CH*CH*, CH$_3$CCH*, and C*C* adsorbed on the Ru(111) surface. (ν, δ, ρ, ω, and τ represent the mode of stretching, scissoring, rocking, wagging and twisting, respectively, the subscript of a and s represent the asymmetric and symmetric modes, respectively.)

HC*CH*	Mode	CH$_3$C*CH*	Mode	C*C*	Mode
3053	ν(CH)	3073	ν(CH$_3$)	1230	ν(CC)
3022	ν(CH)	3041	ν(CH$_3$)		
1085	ν(CC)	3019	ν(CH$_3$)		
852		2999	ν(CH)		
849		1446	δ_a(CH$_3$)		
765	δ(both CH)	1437	δ_a(CH$_3$)		
		1355	δ_s(CH$_3$)		
		1161	δ_a(both CC)		
		1077			
		978			
		960			
		819	δ_s(both CC)		
		812			

References

1   C. K. Ande, S. D. Elliott and W. M. M. Kessels, *J. Phys. Chem. C*, 2014, **118**, 26683-26694.

2   Y. Urashima, T. Wakabayashi, T. Masaki and Y. Terasaki, *Mineral. J.*, 1974, **7**, 438-444.